Sn(III) and Ge(III) in the Thiophenolato-Bridged Complexes $[LFeSnFeL]^{n+}$ and $[LFeGeFeL]^{n+}$ ($n = 2, 3$; L = 1,4,7-(4-*tert*-Butyl-2-mercaptobenzyl)-1,4,7-triazacyclononane)

Thorsten Glaser,[†] Eckhard Bill,[†] Thomas Weyhermüller,[†] Wolfram Meyer-Klaucke,[‡] and Karl Wieghardt*[,†]

Contribution from the Max-Planck-Institut für Strahlenchemie, Stiftstrasse 34-36, D-45470 Mülheim an der Ruhr, Germany, and the European Molecular Biology Laboratory, Outstation Hamburg, D-22603 Hamburg, Germany

Received February 18, 1999

The reaction of mononuclear [LFe^{III}] where L represents the trianionic ligand 1,4,7-tris(4-*tert*-butyl-2-mercaptobenzyl)-1,4,7-triazacyclononane with $Pb(ClO_4)_2 \cdot 3H_2O$ in methanol affords the heterotrinuclear complex $[LFePbFeL](ClO_4)_2$ (**1**). Similarly, with $SnSO_4$ or GeI_2 as starting material in an acetonitrile/water mixture and CH_2Cl_2, respectively, the reaction with [LFe^{III}] yields crystalline materials of $[LFeSnFeL](PF_6)_2$ (**2a**) and $[LFeGeFeL](PF_6)_2$ (**3a**) upon addition of $NaPF_6$. Complexes **2a** and **3a** can be one-electron oxidized by $[Ni^{III}(tacn)_2](ClO_4)_3$ (tacn = 1,4,7-triazacyclononane) to give $[LFeSnFeL](ClO_4)_3$ (**2b**) and $[LFeGeFeL](ClO_4)_3$ (**3b**). The crystal structures of $[LFeSnFeL](BPh_4)_2 \cdot 6CH_3CN$ (**2a***), $[LFeSnFeL](ClO_4)_3 \cdot 4.5(CH_3)_2CO$ (**2b***), and $[LFeGeFeL](BPh_4)_2 \cdot 6CH_3CN$ (**3a***) have been determined by single-crystal X-ray crystallography. The trinuclear cations consist of three face-sharing octahedra connected by six thiolato bridges affording the core $N_3Fe(\mu\text{-}S)_3M(\mu\text{-}S)_3FeN_3$ (M = Sn,Ge). Fe and Sn(Ge) K edge X-ray absorption spectroscopy on **2a**, **2b**, and **3a**, **3b** established that the one-electron oxidations affect exclusively the iron ions whereas the oxidation state of the central Sn(Ge) remains unaffected. $^{119}Sn(^{57}Fe)$ Mössbauer spectroscopy, magnetochemistry, and EPR spectroscopy prove that both the Sn and Ge ions in the di- and trications are *trivalent* since the unpaired electron in **2b** and **3b** displays substantial 5s and 4s character, respectively. In contrast, in **1**, an oxidation state distribution of $l.s.Fe^{III}Pb^{II}l.s.Fe^{III}$ prevails. Complexes **1**, **2a**, and **3a** possess a diamagnetic ground state whereas **2b** and **3b** have an $S_t = {}^1/_2$ ground state.

Introduction

In a series of papers[1−4] we have recently explored the electronic structure of an isostructural class of homo- and heterotrinuclear transition metal complexes all of which contain the thiolato-bridged $N_3M^1(\mu\text{-}SR)_3M^2(\mu\text{-}SR)_3M^3N_3^{n+}$ core which consists of three face-sharing octahedra (Chart 1). With M^1 and M^3 representing two low-spin ferric ions (d^5, $S = {}^1/_2$) in the two terminal positions, in a *fac*-N_3S_3 donor environment, and M^2 a diamagnetic or paramagnetic central heterometal ion in an S_6 ligand sphere we showed that the mechanisms of spin coupling between two or three paramagnetic ions cannot be described exclusively in terms of a classical superexchange model by using the Heisenberg, Dirac, van Vleck (HDvV) spin Hamiltonian[5] for strictly localized valences but spin dependent delocalization via double exchange mechanisms[6] had to be invoked.

We verified the notion that dominant double exchange in *dinuclear* mixed valent species yields an electronic ground state of *maximum spin multiplicity* via spin alignment (ferromagnetic coupling) whereas the situation for trinuclear species is more complicated[7] and a ground state of *minimum spin multiplicity* can be energetically more favorable than its corresponding S_{max} state. For example, in the isoelectronic and isostructural series of complexes $[\{LFe\}_2M^2]^{n+}$ where M^2 ($n+$) is Fe(2) **A**, Co^{III}(3) **B**, Ni(4) **C**, we found that **A** and **B** have an $S_{t,max} = 1$, whereas **C** has an $S_{t,min} = 0$ ground state (LH_3 = 1,4,7-tris(4-*tert*-butyl-2-mercaptobenzyl)-1,4,7-triazacyclononane). We showed[2] that **A** and **C** can only be described with delocalized valences (class III according to Robin and Day[8]) whereas **B** is a class I or II species with localized valences. Formally, all three can in a first approximation be described as consisting of two low-spin ferric ions with $S = {}^1/_2$ and a central diamagnetic, low-spin ferrous ion (d^6, $S = 0$) in **A**, a low-spin cobalt(III) (d^6, $S = 0$) in **B**, and a low-spin Ni(IV) (d^6, $S = 0$) in **C**; they are

[†] Max-Planck-Institut für Strahlenchemie.
[‡] European Molecular Biology Laboratory.

(1) Beissel, T.; Birkelbach, F.; Bill, E.; Glaser, T.; Kesting, F.; Krebs, C.; Weyhermüller, T.; Wieghardt, K.; Butzlaff, C.; Trautwein, A. X. *J. Am. Chem. Soc.* **1996**, *118*, 12376.
(2) Glaser, T.; Beissel, T.; Bill, E.; Weyhermüller, T.; Schünemann, V.; Meyer-Klaucke, W.; Trautwein, A. X.; Wieghardt, K. *J. Am. Chem. Soc.* **1999**, *121*, 2193.
(3) Glaser, T.; Kesting, F.; Beissel, T.; Bill, E.; Weyhermüller, T.; Meyer-Klaucke, W.; Wieghardt, K. *Inorg. Chem.* **1999**, *38*, 722.
(4) Glaser, T.; Wieghardt, K. in *Spectroscopic Methods in Bioinorganic Chemistry*, Solomon, E. I., Hodgson, K. O., Eds.; ACS Symposium Series 692; American Chemical Society: Washington, DC, 1998; p 314.
(5) Kahn, O. *Molecular Magnetism*; VCH Publishers: New York, 1993.
(6) (a) Zener, C. *Phys. Rev.* **1951**, *82*, 403. (b) Anderson, P. W.; Hasegawa, H. *Phys. Rev.* **1955**, *100*, 675. (c) Blondin, G.; Girerd, J.-J. *Chem. Rev.* **1990**, *90*, 1359 and references therein.
(7) (a) Belinskii, M. I. *Mol. Phys.* **1987**, *60*, 793. (b) Borrás-Almenar, J. J.; Coronado, E.; Tsukerblat, B. S.; Georges, R. In *Molecular Magnetism: From Molecular Assemblies to the Devices*; Coronado, E., Ed.; Kluwer: Dordrecht, The Netherlands, 1996; 105. (c) Borrás-Almenar, J. J.; Clemente, J. M.; Coronado, E.; Palii, A. V.; Tsukerblat, B. S.; Georges, R. *J. Chem. Phys.* **1996**, *105*, 6892.
(8) Robin, M. B.; Day, P. *Adv. Inorg. Chem. Radiochem.* **1967**, *10*, 247.

10.1021/ic9902018 CCC: $18.00
Published on Web 05/01/1999

Chart 1

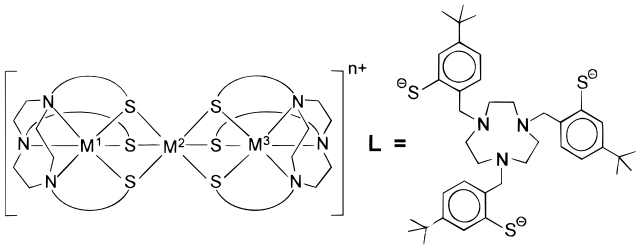

$[LM^1M^2M^3L]^{n+}$ Complexes						
	$M^1 = M^3$	M^2	n	$S_{t,\,max}$ [a]	$S_{t,\,min}$ [a]	Ref.
A	Fe	Fe	2	1		2
	Fe	Fe	3		1/2	2
	Fe	Co^{III}	2		1/2	2
B	Fe	Co^{III}	3	1		2
	Fe	Cr^{III}	1		3/2	2
	Fe	Cr^{III}	2	2		2
	Fe	Cr^{III}	3		1/2	2
	Fe	Ni	2		0	3
	Fe	Ni	3		1/2	3
C	Fe	Ni	4		0	3
1a	Fe	Pb	2		0	this work
2a	Fe	Sn	2		0	this work
2b	Fe	Sn	3		1/2	this work
3a	Fe	Ge	2		0	this work
3b	Fe	Ge	3		1/2	this work

[a] electronic ground state of the respective trinuclear cation

isoelectronic l.s.d^5-l.s.d^6-l.s.d^5 species where parallel spin alignment yields an $S_{t,max} = 1$ ground state and antiparallel an $S_{t,min} = 0$.

In this paper we report our results on a system of similar complexes but where the central metal ion M^2 is a main group ion of germanium, tin, and lead. We reasoned that these ions do not possess energetically low-lying d orbitals via which spin coupling is mediated in the above species. In addition, we anticipated a clear-cut, unambiguous oxidation state assignment of either +II or +IV for the central Ge, Sn, or Pb ion in such $[LFeM^2FeL]^{n+}$ complexes ($n = 2, 3$) and, consequently, a localized model to be applicable (irrespective of the charge n of the species) because the spin carrying Fe ions are separated by 6−7 Å. This proved to be incorrect. We show here that, instead, Ge(III) and Sn(III) ions in an octahedral GeS_6 or SnS_6 environment are stable.

Results

Synthesis and Characterization of Complexes. The reaction of mononuclear $[LFe^{III}]$ [9] with $Pb^{II}(ClO_4)_2 \cdot 3H_2O$ (2:1) in refluxing methanol yields a green solution from which a deep-green, microcrystalline solid of $[LFePbFeL](ClO_4)_2$ (**1**) formed upon cooling to ambient temperature. It has not been possible to grow single crystals suitable for X-ray crystallography of **1** because the compound slowly dissociates in most common solvents with formation of [LFe]. Figure 1 shows the electronic spectrum of **1** in CH_3CN which was recorded immediately after dissolution of the complex; the spectrum is not contaminated with the starting material [LFe] but the intensity of the bands decreases by ∼20% within 1 h indicating its relative instability in solution.

Similarly, the reaction of [LFe] with an excess $Sn^{II}(SO_4)$ in an acetonitrile/water mixture yields upon addition of $NaPF_6$ a black precipitate of $[LFeSnFeL](PF_6)_2$ (**2a**). This species can

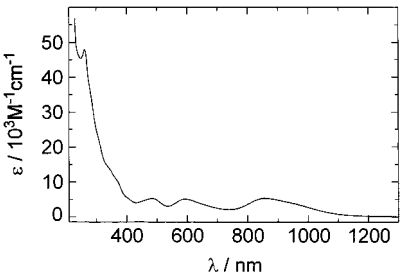

Figure 1. Electronic spectrum of $[LFePbFeL]^{2+}$ (**1**) in acetonitrile.

be one-electron oxidized by 1 equiv of $[Ni^{III}(tacn)_2](ClO_4)_3$[10] in acetone yielding green-black microcrystalline $[LFeSnFeL](ClO_4)_3$ (**2b**). In an analogous fashion the complexes $[LFeGeFeL](PF_6)_2$ (**3a**) and $[LFeGeFeL](ClO_4)_3$ (**3b**) have been prepared from i) the reaction of [LFe] with GeI_2 in CH_2Cl_2 and ii) one-electron oxidation of **3a** with $[Ni^{III}(tacn)_2](ClO_4)_3$ in acetone. All complexes have been characterized by elemental analysis and mass spectrometry where in each case the molecular ion peak $[LFeMFeL]^{2+/3+}$ has been observed (see Experimental Section).

Electrochemistry. The cyclic (cv) and square-wave (swv) voltammograms of complexes in acetonitrile solution containing 0.10 M $[N(n\text{-butyl})_4]PF_6$ as supporting electrolyte have been recorded at a glassy carbon working electrode at ambient temperature. All potentials are referenced versus the ferrocenium/ferrocene couple.

The cv of **1** displays an irreversible oxidation wave at $E_p^{ox} = +0.50$ V and an irreversible reduction at −0.83 V. Consequently, **1** is redox-inactive in the potential range +0.5 to −0.8 V.

In contrast, the cv and swv of **2a** and **3a** display a reversible and a quasireversible one-electron-transfer wave (E^3,E^2) as shown in Figure 2 and an irreversible two-electron reduction wave at quite negative potential, respectively. The redox potentials are given in Table 1. The cvs of **2a**, **2b** and of **3a**, **3b** are identical, respectively. These processes are assigned as shown in Scheme 1. Whereas the di- and tricationic species **2a**, **2b** and **3a**, **3b** are stable species which were isolated as solid materials, the tetracations are only stable in solution on the time scale of a cyclic voltammetric experiment; we have not been able to chemically generate and isolate such species.

It follows from the above experiments that the heterotrinuclear species $[LFeMFeL]^{n+}$ (M = Ge, Sn, but *not* Pb) exist in three different oxidation levels which are interrelated by one-electron-transfer steps without accompanying gross structural changes.

Crystal Structure Determinations. The crystal structures of **2a***, **2b***, and **3a*** have been determined by X-ray crystallography. All three structures consist of heterotrinuclear di- or trications $[LFeMFeL]^{2+/3+}$, well-separated tetraphenylborate or perchlorate anions, and solvent molecules (acetonitrile or acetone). Figure 3 displays the structure of the cation in crystals of **2b***; those in crystals of **2a***, **3a*** are very similar and not shown. All cations possess crystallographically imposed C_i symmetry; in crystals of **2b*** there are two crystallographically independent cations of similar dimensions. All cations have idealized S_6 symmetry; considering the metal ions within their respective first coordination spheres only idealized D_{3d} symmetry prevails. The terminal iron ions are in a distorted octahedral *cis*-N_3S_3 environment of local C_{3v} symmetry whereas the central Sn or Ge ions are in a distorted octahedral S_6 donor

(9) Beissel, T.; Bürger, K. S.; Voigt, G.; Wieghardt, K.; Butzlaff, C.; Trautwein, A. X. *Inorg. Chem.* **1993**, *32*, 124.

(10) Wieghardt, K.; Walz, W.; Nuber, B.; Weiss, J.; Ozarowski, A.; Stratemeier, H.; Reinen, D. *Inorg. Chem.* **1986**, *25*, 1650.

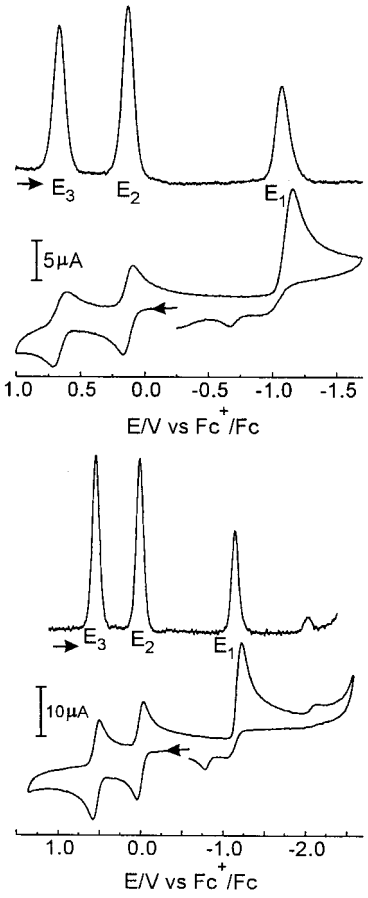

Figure 2. Square-wave and cyclic voltammograms of **2a** (top) and **3a** (bottom). Conditions: CH_3CN solution (0.10 M $[N(n\text{-butyl})_4]PF_6$), 25 °C, glassy carbon working electrode; cv, scan rate 200 mV s^{-1}; swv, frequency, 30 Hz; pulse height, 25 mV.

Table 1. Summary of Redox Potentials of Complexes[a]

complex	$E_p^{red}(E_1)$, V	$E^2_{1/2}$, V	$E^3_{1/2}$, V
2a, **2b**	−1.22	0.07	0.61
3a, **3b**	−1.15	0.01	0.54

[a] Potentials are referenced vs Fc^+/Fc. [b] Conditions: acetonitrile solution 0.10 M $[N(n\text{-butyl})_4]PF_6$; 25 °C; glassy carbon working electrode; cv, scan rate 200 mV s^{-1}; swv, frequency 30 Hz; pulse height 25 mV.

Scheme 1

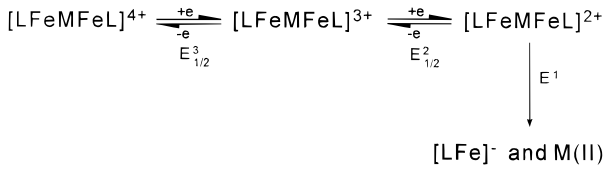

atom coordination sphere, respectively. The stereochemistry of these trinuclear cations has been discussed previously.[1] Only the staggered configuration of the tertiary butyl groups in the achiral stereoisomer $\Delta(\lambda\lambda\lambda)\cdots\Lambda(\delta\delta\delta)$ leads to a stable, sterically not crowded structure.

Table 2 summarizes selected bond distances and angles of the $N_3Fe(\mu\text{-}S)_3M(\mu\text{-}S)_3FeN_3$ cores. Remarkably, the average Fe−N and Fe−S bond distances at 2.038(1) Å and 2.264(1) Å, respectively, are within experimental error identical in all three cations and are indicative of a low-spin configuration at the iron ion with empty e_g* orbitals in O_h symmetry. The average Sn−S bonds in **2a*** and **2b*** at 2.606(1) Å and 2.630(2) Å, respectively, are slightly different. Interestingly, these distances

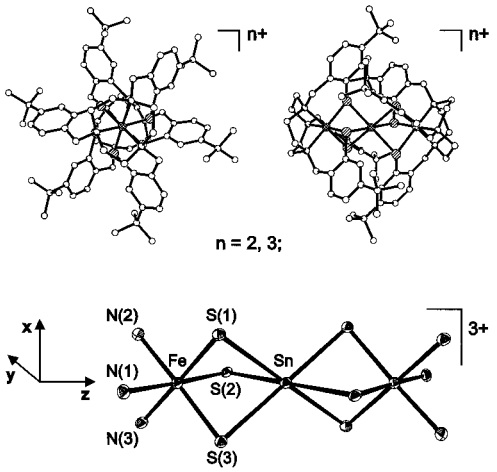

Figure 3. Structure of the trication in crystals of **2b***. (Top Left) View down the Fe−Sn−Fe axis. (Top Right) Side view. (Bottom) Metal ions with their donor atoms. The structures of **2a*** and **3a*** are similar and not shown.

Table 2. Selected Bond Distances (Å) and Angles (deg)

	2a*	**2b***[a]		**3a***
Fe···M	3.270(1)	3.248(1)	3.278(1)	3.093(1)
Fe−S1	2.267(1)	2.253(2)	2.254(2)	2.248(2)
Fe−S2	2.263(1)	2.258(2)	2.250(2)	2.252(2)
Fe−S3	2.262(1)	2.260(2)	2.267(2)	2.246(2)
Fe−N1	2.034(2)	2.034(5)	2.049(5)	2.032(6)
Fe−N2	2.040(2)	2.045(5)	2.038(5)	2.048(6)
Fe−N3	2.041(2)	2.044(5)	2.038(5)	2.046(6)
M−S1	2.607(1)	2.613(1)	2.635(1)	2.433(2)
M−S2	2.608(1)	2.635(1)	2.638(1)	2.438(2)
M−S3	2.603(1)	2.621(1)	2.641(1)	2.422(2)
M−S1−Fe	83.97(2)	83.40(5)	83.84(5)	82.62(6)
M−S2−Fe	84.04(2)	82.81(5)	83.83(5)	82.42(6)
M−S3−Fe	84.16(2)	83.08(5)	83.45(5)	82.90(6)

[a] There are two crystallographically independent trications in the unit cell.

are slightly *longer* in the trication than in the dication. In the crystallographically characterized structure of $[(H_2O)_9Mo_3S_4\text{-}SnS_4Mo_3(H_2O)_9](CH_3C_6H_4SO_3)_8\cdot 26H_2O$ containing an SnS_6 octahedron, the average Sn−S distance is observed at 2.627(3) Å.[11] The authors of this paper have tentatively assigned the central tin ion an oxidation state of +IV. It is also quite interesting that the Fe···Sn distances in the di- and trication are very similar (average 3.265(1) Å). In contrast, in the series $[LFeCo^{III}FeL]^{2+,3+}$ or $[LFeCr^{III}FeL]^{+,2+,3+}$ the Fe···Co or Fe···Cr distances *decrease* with increasing oxidation level.[2]

The germanium ion in **3a*** is also six-coordinate with an average Ge−S distance of 2.431(2) Å and an Fe···Ge distance of 3.093(1) Å.

The above structural parameters do not allow an unambiguous assignment of oxidation states to individual metal ions in the di- or trications. Thus distributions for $[LFeSnFeL]^{2+}$ as $l.s.Fe^{III}\text{-}Sn^{II}l.s.Fe^{III}$ or $l.s.Fe^{II}Sn^{IV}l.s.Fe^{II}$ or even $Fe^{2.5}Sn^{III}Fe^{2.5}$ are conceivable whereas for $[LFeSnFeL]^{3+}$ distributions as $l.s.Fe^{III}\text{-}Sn^{III}l.s.Fe^{III}$ or $l.s.Fe^{III}Sn^{IV}Fe^{II}$ or $l.s.Fe^{III}Sn^{II}l.s.Fe^{IV}$ appear to be reasonable possibilities. The same is true for **3a**, **3b**.

XANES Spectroscopy. The X-ray absorption near edge spectra (XANES) of **2a**, **2b** and **3a**, **3b** have been recorded at the Fe *and* Sn or Ge K edge, respectively. XAS as an element specific spectroscopy allows to analyze the oxidation state of a given element in a coordination compound. The position and

(11) Akashi, H.; Shibahara, T. *Inorg. Chem.* **1989**, *28*, 2907.

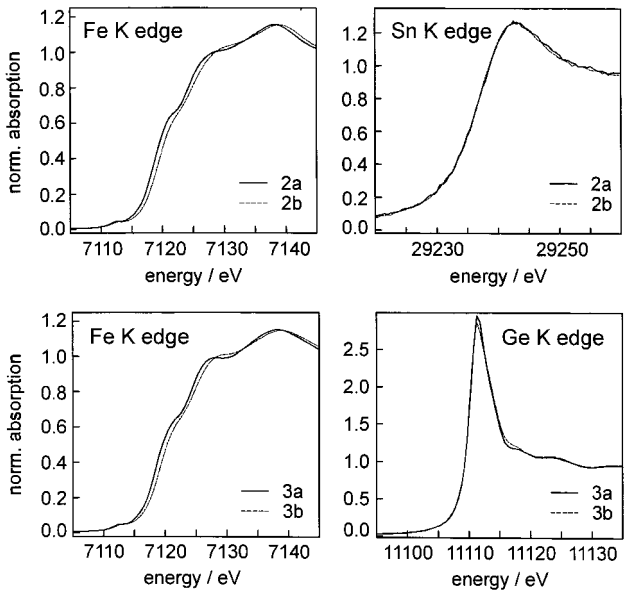

Figure 4. Fe (left) and Sn(Ge) (right) K edge XANES spectra of **2a**, **2b** (top) and **3a**, **3b** (bottom).

Table 3. XANES Results[a]

	Fe K edge, eV	Sn K edge, eV	Ge K edge, eV
2a	7119.68(5)	29234.3(1)	
2b	7120.44(5)	29234.4(1)	
3a	7119.61(5)		11108.2(1)
3b	7120.35(5)		11108.3(1)

[a] Edge positions determined from the maximum of the first derivative of the rising K edge region.

intensity of the resonances and, in particular, the energy of the absorption edge position are features which depend on the electron configuration. We have determined the edge positions from the maximum of the first derivative of the data in the rising edge region.[12] The Fe K edge spectra of **2a**, **2b** and **3a**, **3b** as well as the corresponding Sn, Ge K edge spectra are shown in Figure 4, and the energies of the edge positions are summarized in Table 3.

An important result is the observation that the spectra at both the Fe *and* Sn/Ge K edge of **2a**, **2b** on one hand and of **3a**, **3b** on the other are very similar with respect to shape and intensity. The only significant difference between the spectra of the di- and the tricationic species occurs at the energy of the rising Fe K edge region. In both instances, namely **2a**, **2b** and **3a**, **3b**, the one-electron oxidation yields an energy upshift of ~0.75 eV at the Fe K edge position whereas the Sn and Ge K edge positions remain the same. This is a clear indication that one-electron oxidation of **2a** to **2b** and **3a** to **3b** affects *only* the iron ions and not the central tin or germanium ion. The latter must therefore have a common electron configuration and, hence, the same formal oxidation state.

Magnetic Susceptibility Measurements and EPR Spectroscopy. We have measured the magnetic susceptibility of complexes in the temperature range 2−300 K by using a SQUID-magnetometer. The raw data were corrected for underlying diamagnetism by using tabulated Pascal's constants. Temperature-independent paramagnetism, χ_{TIP}, is a fit parameter as well as a small amount of a paramagnetic impurity, p.i. ([LFe] $S = {}^5/_2$). Plots of χ_M and μ_{eff} vs T and their fits are shown in Figure S1; the results are given in Table 4.

Table 4. Results of the Magnetic Susceptibility Measurements

complex	χ_{TIP}, 10^6 cm^3 mol^{-1} [a]	p.i., %[b]	μ_{eff},μ_B[c]	S_t[d]	g[e]
2a	690	0.5		0	
2b	670	0	1.84	$^1/_2$	2.12
3a	220	0.3		0	
3b	730	0	1.75	$^1/_2$	2.02

[a] Temperature-independent paramagnetism (fit parameter). [b] Paramagnetic impurity ($S = {}^5/_2$) in %. [c] Effective magnetic moment. [d] Spin ground state. [e] g value (fit parameter).

From the magnetic susceptibility data of **1** we conclude that this complex is essentially diamagnetic ($S_t = 0$), although the actual measurements were found to be somewhat dependent on the preparation of the sample. Thus more crystalline samples showed a small increase of μ_{eff} at temperatures >240 K to ~1.3 μ_B at 300 K. In more microcrystalline samples this effect is absent. It is noted that similar effects have been described for [LFe] where a sample-dependent high-spin ($S = {}^5/_2$)−low-spin ($S = {}^1/_2$) equilibrium in the solid state is observed.[9,13]

Complexes **2b** and **3b** clearly possess an $S_t = {}^1/_2$ ground state, as temperature-independent magnetic moments of 1.84 μ_B for **2b** and 1.75 μ_B for **3b** are observed. Species **2a** and **3a** on the other hand have an $S_t = 0$ ground state.

Figure 5 shows the EPR spectra of frozen acetonitrile solutions of **2b** recorded in Q (at 13 K), X (at 10 K), and S band (at 22 K). The X and Q band spectra show resonances for $g_{||}$ and $g_\perp$ of an $S_t = {}^1/_2$ system and, in addition, a doublet at $g_\perp$ with a 56.5 mT hyperfine splitting (X band) which in Q band increases to 69.0 mT. In S band also $g_\perp$ and $g_{||}$ are observed but instead of a simple doublet several additional resonances are detected.

Since only the tin isotopes ^{119}Sn (8.6% natural abundance) and ^{117}Sn (7.7%) possess a nuclear spin $I = {}^1/_2$ where the magnetic moments of both nuclei differ by only 4.6%[14] we have simulated the EPR spectra by using a Hamiltonian for the spin system $S_t = {}^1/_2$ and $I = {}^1/_2$ where the resonances not belonging to the $S_t = {}^1/_2$ system are due to hyperfine coupling to a nuclear spin $I = {}^1/_2$. The hyperfine splitting of the doublet is ~0.07 cm^{-1}. The Zeeman splitting in Q band is ~1.0 cm^{-1} which is much larger than the hyperfine splitting which can therefore be treated in first-order perturbation. Consequently, the splitting at $g_\perp$ is symmetric. The Zeeman splitting in X band is ~0.3 cm^{-1} and the hyperfine splitting must be treated as a second-order effect. The splitting at $g_\perp$ of the two hyperfine signals is now asymmetric. Finally, in S band the Zeeman splitting at ~0.1 cm^{-1} is of the same order of magnitude as the hyperfine splitting which gives rise to the observed complicated pattern of resonances.

Hyperfine coupling constants of the above order of magnitude are well-known and for the simulation of the X band spectra the Breit-Rabi equation has been frequently used. According to this method the hyperfine splitting is treated as second-order perturbation.[15] Since this approximation does not hold for the

(12) (a) Shadle, E. S.; Hedman, B.; Hodgson, K. O.; Solomon, E. I. *Inorg. Chem.* **1994**, *33*, 4235. (b) Shadle, E. S.; Hedman, B.; Hodgson, K. O.; Solomon, E. I. *J. Am. Chem. Soc.* **1995**, *117*, 2259. (c) Westre, T. E.; Kennepohl, P.; DeWitt, J. G.; Hedman, B.; Hodgson, K. O.; Solomon, E. I. *J. Am. Chem. Soc.* **1997**, *119*, 6297.

(13) Butzlaff, C.; Bill, E.; Meyer, W.; Winkler, H.; Trautwein, A. X.; Beissel, T.; Wieghardt, K. *Hyperfine Interactions* **1994**, *90*, 453.

(14) *Handbook of Chemistry and Physics*, 64th ed.; CRC Press: Boca Raton, FL, 1983; (a) p B-262; (b) p B-245; (c) p B-95.

(15) (a) Breit, G.; Rabi, I. *Phys. Rev.* **1931**, *38*, 2082. (b) Atkins, P. W.; Symons, M. C. R. *The Structure of Inorganic Radicals*, 1st ed.; Elsevier: Amsterdam **1967**, pp 238 and 14. (c) Goodman, B. A.; Raynor, J. B. *Adv. Inorg. Chem., Radiochem.* **1970**, *13*, 135.

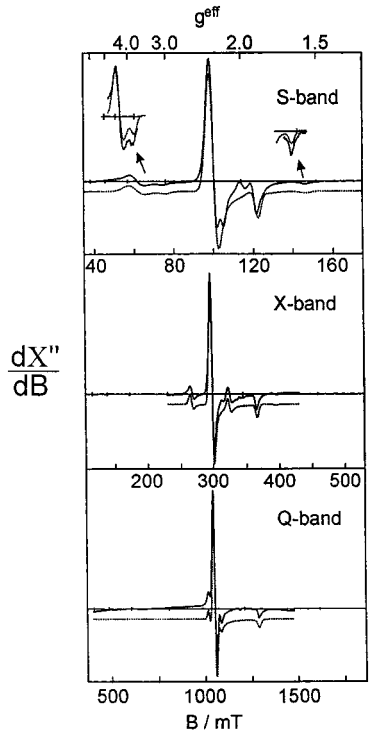

Figure 5. Q (top), X (middle), and S (bottom) band EPR spectra of **2b** in CH_3CN at 13, 10, and 22 K, respectively. Solid lines are experimental spectra; dotted lines are simulations. Conditions: (i) Q band: frequency, 33.898 GHz; power, 92 μW; modulation amplitude, 2.6 mT; modulation frequency, 100 kHz; line width, Γ = (17.2, 17.2, 25.5) mT. (ii) X band: 9.6477 GHz; 200 μW; 1.14 mT; 100 kHz, Γ = (6.9, 6.9, 6.7) mT. (iii) S band: 3.1851 GHz; 1.0 mW; 1.36 mT; 100 kHz; Γ = (9.7, 9.7, 7.0) mT. The insets in the S band spectra are shown with a horizontal compression by a factor of 2 and a vertical expansion by a factor of 8.

present S band spectrum, we have employed a full-matrix diagonalization of the spin Hamiltonian consisting of an electron Zeeman and a hyperfine term.[16] It has been possible to simulate the frequency dependence of the EPR spectra of **2b** successfully by using the following set of parameters: $A_\perp = 620 \times 10^{-4}$ cm^{-1} (1860 MHz, 57 mT), $A_{||} = 560 \times 10^{-4}$ cm^{-1} (1680 MHz, 64 mT), $g_\perp = 2.32$, $g_{||} = 1.88$. The signs of the hyperfine coupling constants remain undetermined. The hyperfine splitting due to the ^{119}Sn and ^{117}Sn isotopes was not resolved.

As we will show below it is reasonable that the trication in **2b** possesses a ground-state configuration comprising two low-spin ferric ions ($S_i = {}^1/_2$) and a Sn(III) ion: [l.s.$Fe^{III}Sn^{III}$-l.s.Fe^{III}]$^{3+}$. There are two possible doublet ground-state configurations possible: $|{}^1/_2;1>$ and $|{}^1/_2;0>$. The corresponding spin projection formulas are given in eqs 1 and 2. The negative sign

$$|{}^1/_2;1> \quad A^{Fe}_{S_t=1/2} = {}^2/_3 a_{Fe} \quad A^{Sn}_{S_t=1/2} = -{}^1/_3 a_{Sn} \qquad (1)$$

$$|{}^1/_2;0> \quad A^{Fe}_{S_t=1/2} = 0 \qquad A^{Sn}_{S_t=1/2} = a_{Sn} \qquad (2)$$

of the hyperfine coupling constant of the iron ions (see below) indicates that the ground state of **2b** is $|{}^1/_2;1>$. The effective tin hyperfine coupling constant of $A_{iso} = 60$ mT yields then a value $a_{iso} = 180$ mT for the intrinsic tin hyperfine coupling constant. *This value indicates significant Sn 5s orbital character for the wave function of the unpaired electron in **2b**, it is therefore best described as a Sn(III) containing species.*[17,18]

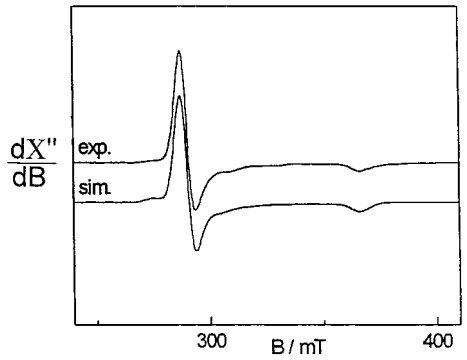

Figure 6. X band EPR spectrum of **3b** in CH_3CN at 4 K. Conditions: frequency 9.4528 GHz; power 20 μW, modulation amplitude 1.97 mT; modulation frequency 100 kHz; simulation with Gaussian lines (Γ = (6.0, 6.0, 8.0) mT).

Figure 6 shows the X band EPR spectrum of a frozen acetonitrile solution of **3b** at 4 K. An axial $S_t = {}^1/_2$ signal and a splitting at $g_\perp$ are observed. The ^{73}Ge isotope (7.8% natural abundance) has a nuclear spin of $I = {}^9/_2$. A simulation of the spectrum for $S_t = {}^1/_2$ and $I = {}^9/_2$ where the hyperfine coupling is treated as second-order perturbation yields the following parameter set: $g_\perp = 2.338$; $g_{||} = 1.843$; $A_{iso} = 34 \times 10^{-4}$ cm^{-1} (3.3 mT; 102 MHz) which gives $g_{iso} = 2.19$. The hyperfine splitting is not resolved due to large line widths. ^{73}Ge hyperfine coupling constants are only $\sim{}^1/_{20}$ of those reported for structurally analogous tin compounds ($^{117/119}$Sn). For example, for $M^{III}(CH(SiMe_3)_2)_3$ these hyperfine coupling constants are 9.2 mT for M = Ge and 169.8 mT for M = Sn.[17e,18e] The ratio of the hyperfine coupling constants **2b**:**3b** of 18:1 is in excellent agreement with this notion. *Consequently, we assign the central germanium ion in **3a** and **3b** on oxidation state of +III.*

Mössbauer Spectroscopy. All new complexes have been extensively studied by ^{57}Fe Mössbauer spectroscopy in zero- and applied magnetic fields. The temperature-dependent zero-field spectra results are summarized in Table 5. The spectra of **1**, **2a**, **2b**, **3a**, and **3b** consist of a single quadrupole doublet in the temperature range 4.2−297 K where the isomer shift is slightly temperature-dependent due to the second-order Doppler effect. The relatively small change of the quadrupole splitting in the same temperature range indicates a very small contribution of the orbital momentum in the ground state. *It is unambiguously established that the two iron sites in each complex are equivalent on the Mössbauer time scale (10^{-7} s) irrespective of the charge of the respective cation (2+ or 3+).*

The diamagnetic ground state of **1**, **2a**, and **3a** has been verified by the spectra in an applied magnetic field at ~4.2 K. These spectra are displayed in Figure 7. The simulations are based on a Hamiltonian described in ref 2. The quadrupole splitting, ΔE_Q, is clearly positive in all cases.

(16) Gaffney, B. J.; Silversone, H. J. *EMR of Paramagnetic Molecules: Biological Magnetic Resonance*; Berliner, L. J., Reuben, J., Eds.; Plenum Press: New York, 1993; adapted and modified by E. Bill (Mülheim).

(17) (a) Bennett, J. E.; Howard, J. A. *Chem. Phys. Lett.* **1972**, *15*, 322. (b) Fieldhouse, S. A.; Lyons, A. R.; Starkie, H. C.; Symons, M. C. R. *J. Chem. Soc., Dalton Trans.* **1974**, 1966. (c) Lassmann, G.; Höppner, K. *Z. Naturforsch. A* **1968**, *23*, 622. (d) Lyons, A. R.; Symons, M. C. R. *J. Am. Chem. Soc.* **1971**, *93*, 7330. (e) Lappert, M. F.; Lednor, P. W. *Adv. Organomet. Chem.* **1976**, *14*, 345.

(18) (a) Davies, A. G. *Adv. Chem. Serv.* **1976**, *157*, 26. (b) Lloyd, R. V.; Rogers, M. T. *J. Am. Chem. Soc.* **1973**, *95*, 2459. (c) Booth, R. J.; Starkie, H. C.; Symons, M. C. R. *J. Phys. Chem.* **1972**, *76*, 141. (d) Davidson, P. J.; Hudson, A.; Lappert, M. F.; Lednor, P. W. *J. Chem. Soc., Chem. Commun.* **1973**, 829. (e) Cotton, J. D.; Cundy, C. S.; Harris, D. H.; Hudson, A.; Lappert, M. F.; Lednor, P. W. *J. Chem. Soc., Chem. Commun.* **1974**, 651. (f) Lappert, M. F.; Powers, P. P. *Adv. Chem. Ser.* **1976**, *157*, 70.

Table 5. Zero-Field ^{57}Fe Mössbauer Parameters of Complexes

complex	T, K	δ, mm s^{-1} [a]	ΔE_Q, mm s^{-1} [b]	Γ, mm s^{-1} [c]
1	4.3	0.35	+1.72	0.25
	80	0.34	+1.72	0.26
	295	0.26	+1.69	0.28
2a	4.2	0.47	+0.51	0.25
	80	0.47	+0.52	0.24
2b	4.3	0.35	+1.56	0.34
	80	0.35	+1.56	0.27
	200	0.32	+1.45	0.29
3a	4.2	0.46	+0.59	0.26
	80	0.45	+0.58	0.27
	297	0.37	+0.62	0.27
3b	4.3	0.34	+1.58	0.32
	80	0.34	+1.49	0.30
	297	0.26	+0.98	0.30

[a] Isomer shift vs α-Fe at 297 K. [b] Quadrupole splitting. [c] Width at half-height.

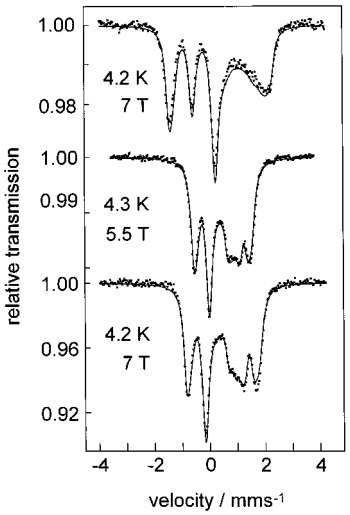

Figure 7. Applied magnetic field Mössbauer spectra of **1** (top), **2a** (middle), and **3a** (bottom) at 4.2 K (7.0 T), 4.3 K (5.5 T), and 4.2 K (7.0 T), respectively. Solid lines represent simulations with a nuclear Hamiltonian without internal magnetic field.

Figure 8 shows the field and temperature-dependent spectra of **2b** which were simulated for an effective spin system $S_t = {}^1/_2$ by using fixed g values from EPR spectroscopy. The fits are not ideal due to the following problem. The internal magnetic field in x,y directions is very small; the A_{xx} and A_{yy} values are close to zero. The fact that the simulations correctly describe the positions of the resonances but not their intensities and line widths, is due to a distribution of A_{zz} values. This is most evident in the 4.2 K and 7 T spectrum. The broadening is mainly located on the higher velocity side which arises from the nuclear transitions to the $m_I = I + -{}^3/_2>$ levels of the excited $I = {}^3/_2$ nuclear state. The effective nuclear g_z value of these levels is larger than that of the other levels. Therefore, this region is very sensitive to variations of A_{zz}. A relative small distribution of A_{zz} leads then to the observed effects. The relaxation is unambiguously determined by the spectrum measured at 200 K. Even at this high temperature the positions of the resonances could be simulated only in the slow relaxation limit. We are aware of only one other example for this effect, namely the NO adduct of myoglobin.[19] The spectrum of **3b** in applied magnetic field is very similar to that of **2b**, it is shown in Figure S2 and the results of the fits are given in Table 6. The simulations in the slow relaxation limit have the same problems

(19) Oosterhuis, W. T.; Lang, G. *J. Chem. Phys.* **1969**, *50*, 4381.

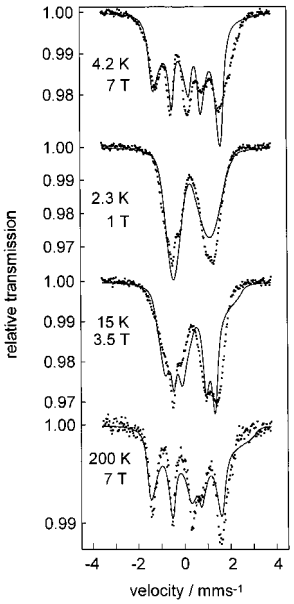

Figure 8. Variable-temperature, variable-field Mössbauer spectra of **2b**. Solid lines represent simulations using parameters given in Table 6.

Table 6. ^{57}Fe Mössbauer Parameters of **2b** and **3b** in Applied Field at 4.2 K

	2b	**3b**
isomer shift, mm s^{-1}	0.35	0.34
quadrupole splitting, mm s^{-1}	+1.56	+1.53
line width at half-height, mm s^{-1}	0.29	0.28
$A_{xx}/\mu_N g_N$, T	−0.47	−4.55
$A_{yy}/\mu_N g_N$, T	−0.47	−4.55
$A_{zz}/\mu_N g_N$, T	−10.38	6.73
$A^{iso}/\mu_N g_N$, T	−3.77	−0.79

as described above for **2b**. A distribution of A_{zz} prevails. The sign of the quadrupole splitting is unambiguously positive, whereas that of A^{iso} is negative.

In a previous paper[2] we have shown that a linear correlation of the isomer shift and the quadrupole splitting of the two terminal iron ions in the isostructural series of complexes $[LFeMFeL]^{+/2+/3+}$ exists where M represents Cr^{III}, Co^{III}, or Fe. This is shown in Figure 9 (top). Gratifyingly, all complexes of the present series containing a central Pb, Sn, or Ge ion fit this correlation well. As we have shown that the oxidation state of the terminal iron ions in $[LFeCo^{III}FeL]^{3+}$, $[LFeCr^{III}FeL]^{3+}$, and $[LFeFeFeL]^{3+}$ is +III (low-spin d^5); in $[LFeCr^{III}FeL]^{2+}$ it is +2.5 and in $[LFeCr^{III}FeL]^{+}$ it is +II (low-spin d^6) the isomer shift obviously also correlates linearly with the oxidation state of these iron ions. Using this correlation one can derive the following oxidation state distributions in the present series of complexes: **1**, $[LFe^{2.9}Pb^{2.2}Fe^{2.9}L]^{2+}$; **2a**, **3a**, $[LFe^{2.3}M^{3.4}Fe^{2.3}L]^{2+}$; and **2b**, **3b**, $[LFe^{2.9}M^{3.3}Fe^{2.9}L]^{3+}$. This is shown in Figure 9 (bottom).

This observation deserves four comments: (i) ^{57}Fe Mössbauer spectroscopy independently shows that whatever the true oxidation state of central Ge or Sn ion is, it must be *the same* for these ions in the di- *and* trications **2a**, **3a** and **2b**, **3b** which is in nice agreement with the Ge, Sn K edge XAS spectra. In other words, one electron oxidation of **2a** to **2b** or **3a** to **3b** affects only the iron ions and not the central Ge or Sn ion. (ii) The ^{57}Fe isomer shifts of **1**, **2b**, and **3b** are very close to the values derived previously for genuine low-spin ferric ions ($\delta = 0.32-0.35$ mm s^{-1}) which out of necessity renders the lead ion in the dication of **1** to be divalent whereas the Ge, Sn ions

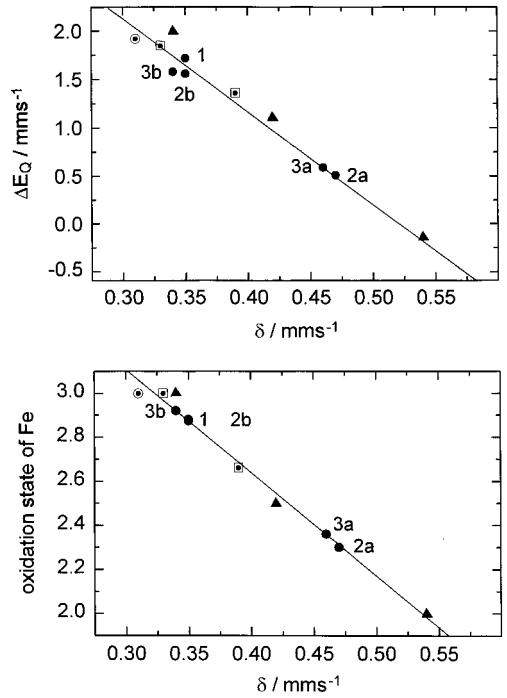

Figure 9. Plot of the isomer shift (at 4.2 K) versus the quadrupole splitting of $[LFeMFeL]^{n+}$ (M = Pb, Sn, Ge) (●), $[LFeCr^{III}FeL]^{+/2+/3+}$ (●), $[LFeCo^{III}Fe^{III}L]^{3+}$ (⊙), and $[LFeFeFeL]^{2+/3+}$ (⊡) complexes (top) and vs the formal oxidation state of the iron ions (bottom) where the present $[LFeMFeL]^{n+}$ complexes (▲) were placed on the straight line in order to determine the formal oxidation state of iron. The line was constructed using values for $[LFeCr^{III}FeL]^{1+/2+/3+}$ (▲), $[Fe^{III}Co^{III}Fe^{III}L]^{3+}$ (⊙) and $[LFeFeFeL]^{2+/3+}$ (⊡) from ref 2 where the formal oxidation state of the iron ions has been spectroscopically determined.

in the trications of **2b** and **3b** must then possess significant *trivalent* character (and in conjunction with i) also in the dications of **2a** and **3a**). (iii) The fact that the above oxidation state distribution involves fractional oxidation states indicates to us that complexes **2a**, **2b**, **3a**, and **3b** are mixed valent species with considerable delocalization of valence electrons over all three ions. (iv) The observation that **1**, **2a**, **2b**, **3a**, and **3b** show the same correlation between the isomer shift and the quadrupole splitting (Figure 9) allows an important conclusion concerning the delocalization pathway to be drawn. The isomer shift yields information about the amount of electron density at the iron sites and the quadrupole splitting, on the other hand, relates to the spatial distribution of the electron density (valence electron contribution to the electric field gradient, EFG). In the series $[LFeMFeL]^{n+}$ with M = Cr, Fe, Co the pathway of electron delocalization is through a direct metal−metal interaction involving the same symmetry allowed mixing of sulfur contribution.[2] Therefore, we conclude that in **1**, **2a**, **2b**, **3a**, and **3b** the same pathway is operative. An interaction between the terminal iron sites involving Fe−S σ/π bonding would disrupt the above correlation (see the series $[LFeNiFeL]^{n+}$ in ref 3).

To probe the oxidation state of the Sn ion in **2a** and **2b** more directly we have also recorded their ^{119}Sn Mössbauer spectra at 77 K.[20] For **2a** an isomer shift, δ, of 2.00 mm s^{-1}, a quadrupole splitting $\Delta E_Q = 0$ mm s^{-1} with a full-line width at half-height $\Gamma = 1.01$ mm s^{-1} has been observed (Figure S3). The isomer shift was referenced versus $CaSnO_3$ at room temperature. Interestingly, the isomer shift of $Sn^{II}S$ is reported at +3.49 mm s^{-1} ($\Delta E_Q = 0.85$ mm s^{-1}) and that of $Sn^{IV}S_2$ at +1.13 mm s^{-1} ($\Delta E_Q = 0$ mm s^{-1}).[21] The isomer shift of **2a** represents nearly the exact arithmetic average between the two values for Sn^{II} and Sn^{IV} and, hence, allows again the assignment of a +III oxidation level of the tin ion in **2a**.

(20) We thank Professor R. Barbieri (Università degli Studi di Palermo) for measuring the ^{119}Sn Mössbauer spectra of **2a** and **2b**.

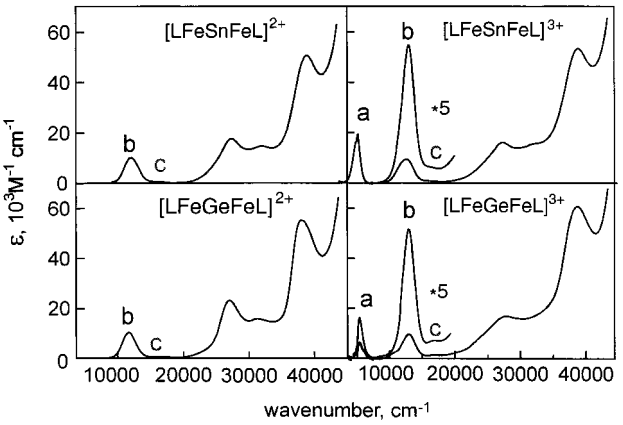

Figure 10. Electronic spectra of **2a**, **2b**, **3a**, and **3b** in CH_3CN at ambient temperature. For the assignment of bands marked a, b, c see text.

Table 7. Sn Hyperfine Coupling Constants

compound	g_{av}	$A_{iso}(^{117}Sn,^{119}Sn)$, mT	ref
Sn^{3+} in solid $SnSO_4$	2.017	885, 930	18c
$Et_3Sn^{\bullet}$	∼2.0	155	17b,e,18b
$Ph_3Sn^{\bullet}$	∼2.0	155	17b,e
$Me_2Sn^{\bullet}Cl$	∼2.0	178	17b
$Sn^{\bullet}(CH(SiMe_3)_2)_3$	2.009	170, 178	18e
$Sn^{\bullet}(N(SiMe_3)_2)_3$	1.991	343, 318	18d−f
$Me_3SnCH_2^{\bullet}$	2.007	13.2	17c
$Et_3SnCH_2CR_2^{\bullet}$	n.d.	40.9	17d
$Cp_2V^{IV}(SnEt_3)Cl$	1.995	19.0	27a
$Cp_2Ti^{III}(SnPh_3)$	1.980	14.6,15.2	27b
$[Ru(SnPh_3)(^iPr\text{-}DAB)]^{-\bullet}$	1.996	31.7, 33.2	26

Despite many attempts and very long exposure times we have not been able to record a ^{119}Sn Mössbauer spectrum of **2b** at 77 K. In *paramagnetic* **2b** the Sn nucleus feels a strong internal magnetic field (see the EPR spectra). Therefore, at very low temperatures in the slow relaxation limit six Sn resonances are expected. With increasing temperature the spin expectation value and the internal field decrease and the 6-line spectrum collapses to a simple quadrupole spectrum where relaxation effects broaden the line widths beyond the detection limit. Due to lack of suitable equipment we have not yet been able to record an ^{119}Sn Mössbauer spectrum in applied field at 4 K.

Electronic Spectra. Figure 10 shows the electronic spectra of complexes, and Table 8 summarizes the observed absorption maxima. The spectra of the dications **2a**, **3a** display two absorption maxima in the visible at ∼610 and ∼840 nm marked c and b, respectively. For **2b** and **3b** the same two bands—slightly shifted to higher energy—are observed but also an additional, new maximum in the near-infrared at ∼1900 nm marked a. The intensity of all of these maxima rules out the assignment as simple d−d transitions of the iron ions.

Discussion

The idealized symmetry of the trinuclear cations is S_6; considering only the metal centers within their first coordination spheres it is D_{3d}. The terminal iron ions in the *fac*-N_3S_3

(21) (a) Hayes, M. C. in *Chemical Applications of Mössbauer Spectroscopy;* Goldanskii, V. I., Herber, R. H., Eds.; Academic Press: New York, 1968; p 314. (b) Boyle, A. J.; Bunburry, D. S. P.; Edwards, C. *Proc. Phys. Soc. (London)* **1962**, *79*, 416.

Table 8. Electronic Spectra of Complexes in CH_3CN Solution at 297 K

complex	λ_{max}, nm (ϵ, L mol^{-1} cm^{-1})
1	262 (4.8×10^4), 485 (5.7×10^3), 592 (5.5×10^3), 853 (5.8×10^3)
2a	257 (5.1×10^4), 313 (1.5×10^4), 365 (1.8×10^4), 610 sh, 834 (1.0×10^3)
2b	257 (5.3×10^4), 313 sh, 365 (1.4×10^4), 610 sh, 770 (1.1×10^4), 1935 (3.8×10^3)
3a	263 (5.5×10^4), 319 (1.6×10^4), 369 (2.3×10^4), 610 (740), 859 (1.0×10^4)
3b	258 (6.1×10^4), 354 (1.6×10^4), 591 (1.4×10^3), 772 (1.0×10^4), 1867 (3.1×10^3)

environment belong to C_{3v} and the central metal ion to point group D_{3d}. Trigonal distortion of a regular octahedral coordination polyhedron affords a splitting of the t_{2g} orbitals (in O_h symmetry) into a doubly degenerate orbital set 1e in C_{3v} and a nondegenerate a_1 orbital. Two directions of this splitting yield then either an $(a_1)^2(1e)^3$ *or* an $(1e)^4(a_1)^1$ electronic configuration for a low-spin ferric ion. The a_1 orbital corresponds to a d_{z^2} orbital where the *z* axis coincides with the 3-fold symmetry axis of the trinuclear cations (Figure 3). The $e(t_{2g})$ orbitals are π orbitals with respect to the metal−ligand bonds and the $e(e_g)$ orbitals are of σ type.[22]

To identify the local magnetic orbital of the ferric ion it is necessary to know the direction of the trigonal splitting. Experimentally, this information is derived from the Mössbauer spectra of **1**, **2a**, **2b**, **3a**, and **3b**. The valence electron contribution to the electric field gradient, $(efg)_{val}$, was estimated by a simple ligand field consideration: the expectation values for the $(efg)_{val}$ tensor elements are known for the individual metal d orbitals.[23] We have recently derived these tensor elements for trigonal symmetry.[24] For a low-spin d^5 system the two above electron configurations $(1e)^4(a_1)^1$ and $(a_1)^2(1e)^3$ give $V_{zz} = +4/7e\langle r^{-3}\rangle$ and $V_{zz} = -2/7e\langle r^{-3}\rangle$, respectively. Therefore, the experimental determination of the sign of the quadrupole splitting by Mössbauer spectroscopy directly yields the respective electron configuration. For all complexes of the present series ΔE_Q is positive and, therefore, $(1e)^4(a_1)^1$ is the electron configuration of all ferric ions; the $a_1(d_{z^2})$ orbital is the magnetic orbital.

The two paramagnetic low-spin ferric ions in **1** are separated via a diamagnetic Pb^{II} ion by at least 6.5 Å and yet **1** has a diamagnetic ground state which is the only populated state up to 295 K. This indicates a strong intramolecular antiferromagnetic coupling between the ferric ions. Using the HDvV Hamiltonian $H = -2JS_1 \cdot S_2$ (with $S_1 = S_2 = {}^1/_2$) we estimate that the coupling constant $|J|$ is larger than 200 cm^{-1}. Since **1** contains two ferric ions with localized valences a superexchange mechanism invoking an antiferromagnetic interaction of the magnetic a_1 orbital with the filled $6s^2$ orbital of the lead ion prevails as shown in Figure 11 where we depict a simplified one-electron MO scheme. Thus the spectroscopic data and the magnetochemistry are in accord with a description of **1** as $l.s.Fe^{III}Pb^{II}l.s.Fe^{III}$ species with localized valences.

The picture is dramatically different for the isostructural and isovalence electronic dications **2a** and **3a** as compared to **1**. Clearly, the tin and germanium ions in **2a** and **3a** are *not* divalent but display trivalent character. Most significantly the ^{57}Fe isomer shift of the *fac*-N_3S_3Fe moieties in **1** on one hand and **2a**, **3a** on the other hand differ; a shift to larger velocities by ∼0.1 mm s^{-1} is observed. In the previous study ref 2 we showed

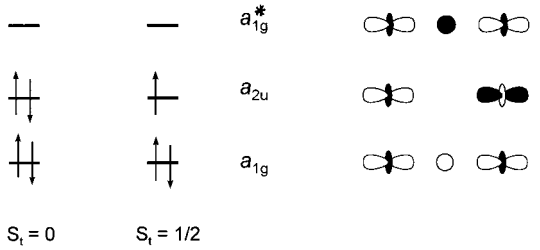

Figure 11. One-electron MO scheme for two atomic a_1 (d_{z^2}) orbitals of iron and an s-orbital of the main group central metal ion in $[LFeMFeL]^{n+}$ complexes giving rise to an $S_t = 0$ ($n = 2$) and $S_t = {}^1/_2$ ($n = 3$) ground state, respectively.

that reduction of $l.s.Fe^{III}$ to the corresponding $l.s.Fe^{II}$ is accompanied by an increase of the isomer shift by ∼0.2 mm s^{-1}. Similarly, a ^{119}Sn isomer shift of 2.00 mm s^{-1} for **2a** is intermediate between typical values found for octahedral Sn(II) compounds (+2.10 to +4.40 mm s^{-1}) and those reported for octahedral Sn(IV) complexes (−0.47 to +1.40 mm s^{-1}).[21] This is also corroborated by the linear relationship between the formal oxidation state of the iron ions and their ^{57}Fe isomer shift as shown in Figure 9 (bottom) which yields an oxidation state distribution in **2a** as $Fe^{2.3}Sn^{3.4}Fe^{2.3}$. Thus the iron ions possess significant divalent and the tin ion trivalent character. Note the same holds true for **3a** for which we deduce an oxidation state distribution of $Fe^{2.4}Ge^{3.2}Fe^{2.4}$.

From the structure determinations it is clear that the Fe−Sn and Fe−Ge distances at 3.270(1) and 3.093(1) Å are in the range for making a direct interaction between the a_1 magnetic orbitals of the Fe ions with the 5s and 4s orbitals of the central tin or germanium ion possible. In an MO description shown in Figure 11 the diamagnetic ground state immediately follows and the Fe−M bonds (M = Sn, Ge) have a formal bond order of 0.5 (3c, 4e bond). Mössbauer spectroscopy implies that these bonds are polar where the two ferric ions accept electron density (∼1e) from the formally divalent Sn or Ge ions rendering them trivalent.

One-electron oxidation of **2a** to **2b** (and **3a** to **3b**) does not affect the Sn or Ge K edge energy but shifts the Fe K edge energy by +0.7 eV. Accordingly, the ^{57}Fe isomer shift decreases by 0.12 mm s^{-1}, respectively. This leads to a formal oxidation state distribution of $Fe^{2.9}Sn(Ge)^{3.3}Fe^{2.9}$ in **2b** (**3b**) using the relationship in Figure 9. Since both **2b** and **3b** are paramagnetic with an $S_t = {}^1/_2$ ground state, EPR spectroscopy is a very powerful tool to interrogate the electronic structure of these compounds and experimentally verify the assignment of a +III oxidation state of the Sn(Ge) ion.

Table 7 summarizes some pertinent Sn hyperfine coupling constants for known Sn(III) compounds (Sn radicals). There are roughly three different classes of paramagnetic tin compounds. (i) The Sn^{3+} ion in an octahedral oxygen environment possesses a very large a_{iso} (^{117}Sn,^{119}Sn) value of ∼900 mT which is characteristic for a $5s^1$ electron configuration.[18c] (ii) more covalent compounds containing formally Sn(III) display a_{iso} values in the range 150−300 mT where the unpaired electron occupies a hybrid orbital with significant 5s contribution (sp^x

(22) Albright, T. A.; Burdett, J. K.; Whangbo, M. H. *Orbital Interactions in Chemistry*; Wiley-Interscience: New York, 1985; p 381.
(23) (a) Trautwein, A. X.; Bill, E.; Bominaar, E. L.; Winkler, H. *Structure and Bonding*; Springer: New York, 1991; Vol. 78, p 1. (b) Gütlich, P. In *Mössbauer Spectroscopy*; Gonser, U., Ed.; Springer: New York, 1975.
(24) Bossek, U.; Nühlen, D.; Bill, E.; Glaser, T.; Wieghardt, K.; Trautwein, A. X. *Inorg. Chem.* **1997**, *36*, 2834.

orbitals) as in organic SnR_3 or $Sn^{III}(N(SiMe_3)_2)_3$ compounds. (iii) Sn(II) or Sn(IV) containing compounds which contain a covalently bound, organic C-centered radical in their vicinity have a_{iso}(Sn) values <40 mT.

Three coordination compounds are also of interest in the above context. The ligand *N*,*N*′-bis(3-carboxysalicylidene)-ethylenediamine forms the bisphenolato-bridged heterodinuclear

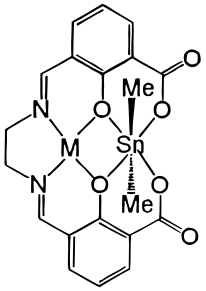

$Co^{II}Sn^{IV}$ and $Cu^{II}Sn^{IV}$ complexes.[25] The unpaired electron is localized at the transition metal ion and despite short $M^{II}\cdots Sn^{IV}$ distances (~2.6 Å) there is no Sn hyperfine coupling observed. In contrast, in $[Ru(SnPh_3)_2(CO)_2(^i$Pr-DAB)$]^{-\cdot}$ there are two covalent Ru−Sn bonds at ~2.69 Å (X-ray structure of the neutral molecule).[26] Its EPR spectrum displays ^{117,119}Sn hyperfine coupling of 31.7 and 33.2 mT. From density functional calculations the authors conclude that the unpaired electron is in a highly delocalized SOMO which allows its accommodation "on the $SnPh_3$, i-Pr-DAB, and, to a lesser extent, CO ligands." Two organometallic species containing the paramagnetic Cp_2Ti^{III} and Cp_2V^{IV} fragments and Ti−SnR_3, V−SnR_3 bonds show similar Sn hyperfine coupling.[27]

Thus the above data clearly support the notion that complexes **2b**, **3b** contain trivalent Sn and Ge ions with a significant degree of $5s^1(4s^1)$ character.

At this point a closer inspection of the electronic spectra of **2a**, **2b** and **3a**, **3b** is rewarding. In Figure 11 a one-electron MO scheme for the di- and trications has been constructed by a linear combination of two $a_1(d_{z^2})$ and an a_1(s) metal orbital of iron and tin (germanium), respectively, which gives rise to an a_{1g} bonding, an a_{2u} nonbonding, and an a^*_{1g} antibonding MO (in D_{3d} symmetry of the trinuclear core structure). This allows the construction of the term scheme shown in Figure 12 for the dications with $S_t = 0$ ground state ($^1A_{1g}$) and for the trications with $S_t = {}^1/_2$ ($^2A_{2u}$). Interestingly, there are two spin and electric dipole allowed transitions for the trications: $^1A_{2u} \rightarrow {}^2A_{1g}$ (a) and $^2A_{2u} \rightarrow {}^2A_{1g}$ (b) and, in addition, a spin-allowed but electric dipole forbidden third transition $^2A_{2u} \rightarrow {}^2A_{2u}$ (c) all of which are observed. In contrast, for the dications only one spin and electric dipole allowed transition b is observed and, in addition, a spin-allowed but electric dipole forbidden transition c. The electric dipole allowed transition b should be polarized in *z* direction (Fe···M···Fe axis). This is indeed the case as single-crystal absorption spectra using polarized light on **2a*** have shown.[28]

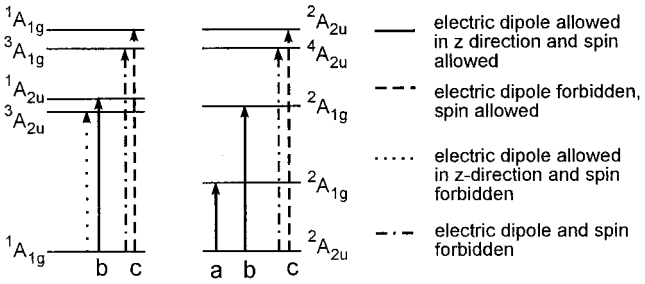

Figure 12. Term schemes for the diamagnetic dications **2a**, **3a** (left) and paramagnetic trications **2b**, **3b** (right). The one-electron transitions marked a, b, and c correspond to the observd absorption maxima in Figure 11.

The simple symmetric one-electron MO scheme in Figure 11 does not account for the experimental observation from EPR spectroscopy of **2b**, **3b** that there is significant spin density at the Sn(Ge) nucleus. If the a_{2u} orbital (Figure 11) is truely nonbonding there is a node and, consequently, zero spin density at the central Sn(Ge) ion. In this case the energy differences between the nonbonding a_{2u} and the bonding and antibonding a_{1g} orbitals are the same. In a term scheme neglecting electron relaxation (Figure 12, right-hand side) this would result in a degeneracy of the two $^2A_{1g}$ states. The electronic spectra of **2b** and **3b** clearly show that this is not the case; the a_{2u} orbital has significant bonding character leading to spin density at the Sn-(Ge) nucleus.

Conclusions

We have synthesized an isostructural series of heterotrinuclear complexes **1**, **2a**, **2b**, **3a**, **3b** where the central ion is lead, tin, or germanium and the two terminal ions are low-spin iron. The electronic structure of each of these species has been elucidated by a combination of spectroscopic methods (^{57}Fe and ^{119}Sn Mössbauer; X, S, and Q band EPR; Fe, Sn, and Ge K edge XAS; UV−vis−NIR) and magnetochemistry.

For **1** containing a trinuclear dication an oxidation state distribution of $l.s.Fe^{III}Pb^{II}l.s.Fe^{III}$ prevails. Superexchange coupling via the a_1 magnetic orbitals of the ferric ions and the $6s^2$ valence electrons of the lead ion yields a diamagnetic ground state. The intramolecular coupling is very strong.

In contrast, the corresponding isostructural and isoelectronic dications in **2a** and **3a** cannot be described as $l.s.Fe^{III}M^{II}l.s.Fe^{III}$ species but are mixed valent species with a formal oxidation state distribution $l.s.Fe^{2.4}Sn^{3.2}l.s.Fe^{2.4}$. In other words, the onset of Fe−Sn or Fe−Ge metal−metal bonding via the a_1 orbitals of the iron ion and the 5s or 4s orbitals of Sn or Ge yields a very weak 3c, 4e bonding situation with a diamagnetic ground state.

One-electron oxidation of **2a**, **3a** yielding the tricationic species **2b** and **3b** affects only the iron centers and not the respective central main group ion which possesses formally a +III oxidation state. An oxidation state distribution of $l.s.Fe^{2.9}Sn^{3.2}(Ge^{3.3})l.s.Fe^{2.9}$ can be envisaged in the trications yielding an $S_t = {}^1/_2$ ground state. It is shown that the unpaired electron has substantial 5s or 4s character. In an MO description the onset of a 3c, 3e bonding situation between the two iron ions and an Sn or Ge ion is proposed.

Experimental Section

Preparation of Complexes. ***Safety Note.*** *Although we have not encountered any problems, it is noted that perchlorate salts of metal complexes with organic ligands are potentially explosive. Only small*

(25) Shindo, K.; Okawa, H.; Aratake, Y.; Kida, S. *Inorg. Chim. Acta* **1991**, *180*, 47.
(26) Aarnts, M. P.; Wilms, M. P.; Peelen, K.; Fraanje, J.; Goubitz, K.; Hartl, F.; Stufkens, D. J.; Baerends, E. J.; Vlcek, A., Jr. *Inorg. Chem.* **1996**, *35*, 5468.
(27) (a) Razuvaev, A. G. C.; Abkumov, G. A.; Gladyshev, E. N.; Fokeev, A. P.; Cherkasov, U. K. *Dokl. Akad. Nauk. SSSR* **1982**, *266*, 135. (b) Kenworthy, J. G.; Myatt, J. *J. Chem. Soc., Chem. Commun.* **1970**, 447.
(28) We thank Dr. T. Brunold (Stanford University) for measuring the single-crystal polarized absorption spectra.

Table 9. Crystallographic Data for **2a**·6MeCN, **2b**·4.5acetone, and **3**·6MeCN

	2a*	2b*	3a*
chem formula	$C_{138}H_{166}B_2Fe_2N_{12}S_6Sn$	$C_{91.5}H_{135}Cl_3Fe_2N_6O_{16.5}S_6Sn$	$C_{138}H_{166}B_2Fe_2N_{12}S_6Ge$
fw	2437.20	2112.16	2391.10
space group	$P\bar{1}$	$P\bar{1}$	$P\bar{1}$
a, Å	13.609(1)	15.772(2)	13.531(1)
b, Å	16.598(2)	17.527(2)	16.578(2)
c, Å	17.302(2)	20.096(3)	17.199(2)
α, deg	100.35(2)	72.95(2)	100.06(2)
β, deg	111.26(2)	79.09(2)	112.15(2)
γ, deg	111.67(2)	68.50(2)	112.01(2)
V, Å	3155.1(8)	4920.4(12)	3080.3(5)
Z	1	2	1
T, K	173	173	100
diffractometer	Siemens SMART CCD	Siemens SMART CCD	Siemens SMART CCD
radiation *λ*, Å	0.710 73	0.710 73	0.710 73
ρ calcd, g cm^{-3}	1.283	1.426	1.289
μ(Mo Kα), cm^{-1}	5.78	8.17	6.33
R1[a] [$I > 2\sigma(I)$]	0.0438	0.0558	0.0792
WR2[b] [$I > 2\sigma(I)$]	0.1086	0.1098	0.1366

[a] $R1 = \sum||F_o| - |F_c||/\sum|F_o|$. [b] $wR2 = [\sum[w(F_o^2 - F_c^2)^2]/\sum[w(F_o^2)^2]]^{1/2}$, where $w = 1/\sigma^2(F_o^2) + (aP)^2 + bP$, $P = (F_o^2 + 2F_c^2)/3$.

amounts of material should be prepared which must be handled with great care and appropriate precautions.

[LFePbFeL](ClO$_4$)$_2$ (1). To an argon-flushed suspension of [LFe^{III}][9] (200 mg; 0.28 mmol) in dry methanol (50 mL) was added Pb(ClO$_4$)$_2$·3H$_2$O (70 mg; 0.15 mmol). The resulting green solution was heated to reflux for 30 min. Upon cooling to room temperature a black, microcrystalline precipitate formed which was filtered off, washed with cold water and diethyl ether and dried in air. Yield: 200 mg (77%). L-SIMS (MNBA) *m/z* (relative intensity, %): 1739.6(0.4) {[LFePbFeL](ClO$_4$)}$^+$, 1640.7(1) {LFePbFeL}$^+$, 924.4(16) {LFeP}$^+$, 716(18) {LFe}$^+$. Anal. Calcd for $C_{78}H_{108}N_6S_6Cl_2O_8Fe_2Pb$: C, 50.9; H, 5.9; N, 4.6; S, 10.5. Found: C, 51.1; H, 6.3; N, 4.3; S, 10.7.

[LFeSnFeL](PF$_6$)$_2$ (2a). To a solution of [LFe] (400 mg; 0.56 mmol) in CH$_3$CN (60 mL) and water (5 mL) was added SnSO$_4$ (2.0 g; 9.3 mmol). The solution was stirred at room temperature for 5 h during which time the solution was twice filtered using blue band quality filters. A filtered solution of NaPF$_6$ (0.5 g) in CH$_3$CN (10 mL) was added and the combined solutions were stored at +4 °C overnight. Black microcrystals of **2a** formed. Workup as described above. Yield: 320 mg (63%). L-SIMS (MNBA) *m/z* (relative intensity, %): 1571.8(0.5) {LFeSnFeLF}$^+$; 1552.8(1) {LFeSnFeL}$^+$; 836.5(13) {LFeSn}$^+$. Anal. Calcd for $C_{78}H_{108}N_6S_6P_2F_{12}Fe_2Sn$: C, 50.8; H, 5.9; N, 4.6; S, 10.4. Found: C, 50.5; H, 5.9; N, 4.4; S, 10.3.

[LFeSnFeL](ClO$_4$)$_3$ (2b). To a solution of **2a** (259 mg; 0.14 mmol) in acetone (50 mL) was added [Ni^{III}(tacn)$_2$](ClO$_4$)$_3$ 10 (87 mg; 0.14 mmol) (tacn = 1,4,7-triazacyclononane). The color of the solution changed within 2 min from green to brownish-green. After stirring for 60 min at ambient temperature and filtration a solution of NaClO$_4$ (500 mg) in acetone (10 mL) was added. Within a few hours at +4 °C a green-black, microcrystalline precipitate formed which was collected by filtration. Workup as described above for **1**. Yield: 160 mg (63%). L-SIMS (MNBA) *m/z* (relative intensity, %): 1751.5(0.8) {LFeSnFeL(PF$_6$)$_2$}$^+$; 1649.5(3.5) {LFeSnFeL(PF$_6$)}$^+$; 1551.3(1) {LFeSnFeL}$^+$; 836.0(67) {LFeSn}$^+$. Anal. Calcd for $C_{78}H_{108}N_6S_6Cl_3O_{12}Fe_2Sn$: C, 50.6; H, 5.9; N, 4.5; S, 10.4. Found: C, 49.9; H, 6.2; N, 4.4; S, 10.2.

[LFeGeFeL](PF$_6$)$_2$ (3a). To an argon flushed solution of [LFe] (350 mg; 0.49 mmol) in CH$_2$Cl$_2$ (40 mL) was added GeI$_2$ (190 mg; 0.58 mmol). The color of the solution changed from blue-green to grass-green. The solution was stirred at 50 °C for 3 h under an argon-blanketing atmosphere. After cooling to 20 °C methanol (20 mL) was added and the solution was filtered. The precipitate formed was discarded. The reaction volume was reduced by one-half by evaporation in a vacuum. A solution of NaPF$_6$ (500 mg) in CH$_3$OH (10 mL) was added dropwise to the filtrate. Within 15 h at 4 °C a black microcrystalline precipitate of **3a** formed which was collected by filtration. Workup as above yield a grass green powder. Yield: 310 mg (70%). Electrospray ionization (ESI) mass spectrum (CH$_3$CN): *m/z* (relative intensity, %): 1605.2(23) {LFeGeFeL(ClO$_4$)}$^+$; 753.2(100) {LFeGeFeL}$^{2+}$.

[LFeGeFeL](ClO$_4$)$_3$ (3b). To a solution of **3a** (220 mg; 0.11 mmol) in acetone (20 mL) was added [Ni^{III}(tacn)$_2$](ClO$_4$)$_3$ (100 mg; 0.16 mmol). The color of the solution changed within 2 min from green to olive green. After stirring for 60 min at ambient temperature the solution was filtered and a solution of NaClO$_4$ (500 mg) in acetone (10 mL) was added. Within a few hours at 4 °C a black microcrystalline precipitate formed which was collected by filtration. Workup as described above for **1** yielded an olive green powder of **3b**. Yield: 150 mg (75%). ESI-MS (CH$_3$CN) *m/z* (relative intensity, %): 1605.5(8) {LFeGeFeL(ClO$_4$)}$^+$; 753.3(100) {LFeGeFeL}$^{2+}$; 502.1(23) {LFeGeFeL}$^{3+}$. Anal. Calcd for $C_{78}H_{108}N_6S_6Cl_3O_{12}Fe_2Ge$: C, 51.9; H, 6.0; N, 4.7; S, 10.7. Found: C, 51.6; H, 6.1; N, 4.8; S, 11.0.

Single crystals suitable for X-ray crystallography were obtained as follows: single crystals of [LFeSnFeL](BPh$_4$)$_2$·6CH$_3$CN (**2a***) grew slowly from a CH$_3$CN/H$_2$O solution containing [LFe] and SnSO$_4$ upon slow diffusion of a CH$_3$CN solution containing Na[BPh$_4$] into the former solution. Crystals of [LFeSnFeL](ClO$_4$)$_3$ 4.5 (CH$_3$)$_2$CO (**2b***) were obtained from an acetone solution of **2b** upon slow evaporation of the solvent. Crystals of [LFeGeFeL](BPh$_4$)$_2$·6CH$_3$CN (**3a***) were obtained from a CH$_3$CN solution of **3a** into which a solution of CH$_3$CN/Na[BPh$_4$] was allowed to slowly diffuse.

X-ray Crystallographic Data Collection and Refinement of the Structures. A black single crystal of **2a***, **2b***, and **3***, respectively, was selected directly from the mother liquor with glass fibers and fixed with a drop of perfluoropolyether. Immediate mounting on a Siemens SMART CCD-detector diffractometer equipped with a cryogenic nitrogen cold stream prevented evaporation of solvent of crystallization. Graphite-monochromated Mo Kα radiation ($\lambda = 0.71073$ Å) was used. Crystallographic data of the compounds are listed in Table 9. Cell constants were obtained from a least-squares fit of a subset of 8192 strong reflections in each case. Intensity data for **2a***, and **2b*** were collected at −100(2) °C, and for **3*** at −173(2) °C, taking frames at 0.30° in Θ. Data were corrected for Lorentz and polarization effects but no absorption correction was carried out due to small absorption coefficients. The Siemens ShelXTL[29] software package was used for solution, refinement and artwork of the structures. All structures were readily solved and refined by direct methods and difference Fourier techniques performed on DEC Alpha workstations. Neutral atom scattering factors were obtained from tables.[30] All non-hydrogen atoms were refined anisotropically except those of disordered perchlorate anions and solvent molecules which were isotropically refined. All hydrogen atoms were placed at calculated positions and refined as riding atoms with isotropic displacement parameters.

(29) *ShelXTL* V.5.03; Siemens Analytical X-ray Instruments, Inc.: Madison, WI, 1995.

(30) *International Tables for X-ray Crystallography*; Kynoch Press: Birmingham, U.K., 1991.

Physical Methods. UV−vis−NIR spectra of CH_3CN solutions of complexes were measured on a Perkin-Elmer Lambda 19 spectrophotometer in the range 210−3200 nm at ambient temperature. Positive ion FAB mass spectra were obtained under the conditions of liquid secondary ion mass spectrometry (L-SIMS) using Cs^+ as the primary ion (22 keV) on a VG autospectrometer with *m*-nitrobenzyl alcohol (MNBA) as the matrix solvent. Cyclic and square-wave voltammetric and controlled potential coulometric measurements were performed on EG&G equipment (potentiostat/galvanostat model 273 A) on Ar-flushed CH_3CN solutions of samples containing 0.10 M $[N(n\text{-but})_4]PF_6$ as supporting electrolyte under an Ar blanketing atmosphere. Potentials were referenced versus the $Ag/AgNO_3$ electrode. Temperature-dependent magnetic susceptibilities of powdered samples were measured by using a SQUID magnetometer (Quantum Design) at 1.0 T in the range 2.0−300 K. For calculations of the molar magnetic susceptibility, χ_M, the raw data were corrected for underlying diamagnetism of the sample by using tabulated Pascal's constants and for the temperature-independent paramagnetism, χ_{TIP}, which was obtained by a fitting procedure. EPR spectra of frozen solutions were recorded on a Bruker ESP 300E spectrometer equipped with a helium flow cryostat (X band, Oxford Instruments ESR 910; S and Q band, Oxford Instruments CF 935). The X band resonator was a dual-mode cavity (Bruker ER 4116 DM/95). The Mössbauer spectra were recorded on an alternating constant-acceleration spectrometer. The minimal line width was 0.24 mm s^{-1} (full width at half-height). The sample temperature was maintained constant either in an Oxford Variox or an Oxford Mössbauer-Spectromag cryostat. The latter is a split-pair superconducting magnet system for applied fields up to 8 T where the temperature of the samples can be varied in the range 1.5−250 K. The field at the samples is oriented perpendicular to the γ-beam. The $^{57}Co/Rh$ source (1.8 GBq) was positioned at room-temperature inside the gap of the magnet system at a zero-field position. ^{57}Fe isomer shifts are referenced relative to α-Fe metal at 295 K. The X-ray absorption spectra (XAS) were recorded at the beam lines E4 and $\times 1.1$ at HASYLAB (DESY, Hamburg, Germany). The beam lines are equipped with three ionization chambers which allow a calibration of each spectrum to a reference sample. The measurements were performed at room temperature. Monochromatization was achieved by a Si(III) monochromator for the Fe and Ge, Sn K edges, respectively. At beam line E4 a focusing mirror is installed in front of the monochromator for further rejection of the harmonics. For suppression of harmonics the monochromator has been detuned to 50% of its peak intensity. Energy calibration was achieved by use of reference samples; for the Fe K edge an α-Fe foil was chosen. This calibration of data has been performed by using WINXAS whereas the normalization and data reduction were done with EXPROG.[31]

Acknowledgment. We thank the Fonds der Chemischen Industrie for financial support of this work.

Supporting Information Available: Figures S1, S2, and S3; tables of crystallographic and crystal structure refinement data, atom coordinates, bond lengths and angles, anisotropic thermal parameters, and calculated positional parameters of hydrogen atoms. This material is available freeof charge via the Internet at http://pubs.acs.org.

IC9902018

(31) (a) Ressler, T. *LLNL, EXAFS program for Windows 3*, Version 2.4. http://ourworld.compuserve.com/homepage/+ressler/. (b) Hermes, C.; Nolting, H. F. *EXAFS data analysis and evaluation program package for PC*; EMBL-Outstation Hamburg: Germany.